ISSN 1810-2328, Journal of Engineering Thermophysics, 2022, Vol. 31, No. 1, pp. 187–199. © Pleiades Publishing, Ltd., 2022.

Numerical Investigation of Corrugated Channel with Backward-Facing Step in Terms of Fluid Flow and Heat Transfer

F. Koca*

Sivas Cumhuriyet University, Faculty of Technology, Department of Manufacturing Engineering, Campus, Sivas, Turkey

Received November 3, 2021; in final form, January 19, 2022; accepted January 20, 2022

Abstract—In this study, the turbulent fluid flow and heat transfer through a backward-facing step connected by various triangles to a corrugated wall were numerically investigated. The governing equation was solved with Ansys Fluent, a CFD (Computational Fluid Dynamic) application that provides solutions using the Finite Volume Method (FVM). The working channel was considered with the step length H and an expansion ratio of 2. While the main channel geometry has a straight bottom surface, the compared channel geometry has a triangular bottom surface with various step lengths (p = 5 mm, p = 10 mm, and p = 15 mm) at a constant amplitude height (5 mm), and a heat flux of 4 kW/m^2 was applied to this surface. The Reynolds number Re was studied in the range of 5000 to 20000. The Performance Evaluation Criterion (PEC) values, which are a function of the Nusselt number Nu and the skin friction, are calculated. As a result, while all the surfaces increase the heat transfer, the highest PEC values are obtained at Re = 5×10^3 and Re = 10^4 in the channel with the 10 mm triangular bottom surface and at Re = 1.5×10^4 and Re = 2×10^4 in the channel with the 20 mm triangular bottom surface.

DOI: 10.1134/S1810232822010143

1. INTRODUCTION

Human beings have been consuming energy resources from past to present. The fact that non-renewable energy resources are limited and their consumption is increasing gradually reveals the necessity of using these resources more effectively. The most important way to achieve this is through the production of more efficient energy systems. Many researchers apply surface modifications to increase the amount of heat transfer with acceptable pressure drop for production of such systems in thermal energy fields. In the literature, these processes with modified surfaces are called passive methods. These methods are frequently applied in the design of heat exchangers used in many fields, from building heating systems to the automotive industry, from the marine to the petrochemical industry. Therefore, the backward-facing step, which has a significant impact on the thermal performance of heat exchanger and the heat transfer mechanism, is of interest to many researchers. The fluid and geometry parameters have been extensively investigated in terms of enhancement of the heat transfer efficiency of backward-facing step applications [1–8]. To quote a few, Ali and Ramadhyani conducted an experimental study to examine the heat transfer in corrugated channels. They performed the research in the $150 < Re < 4000$ range with water as the working fluid. As a result of the experiment, they stated that for $Re > 1500$, the Nusselt numbers in the corrugated channels exceeded those in the parallel plate channel by about 140% and 240% for the two channel spacings. They also showed that the corresponding increases in the friction factor were 130% and 280% [9]. Islamoğlu and Parkazsızoğlu carried out experiments to determine the forced convection heat transfer coefficients and friction factor for air flow in the corrugated channel used in plate heat exchangers. They determined two channel heights of 5 and 10 mm for a single corrugation angle of 20° and performed the experiments in the range of $1200 \leqslant Re \leqslant 4000$. They stated that increasing the channel height resulted in a significant rise in both the Nusselt number and

*E-mail: ferhatkoca@cumhuriyet.edu.tr

the friction factor, but the performance was slightly reduced with respect to the flow area goodness factor [10]. Nalphon studied the heat transfer and pressure drop in a channel under a constant heat flux with V-groove top and bottom plates. He presented corrugated plates with angles of 20°, 40° and 60°, Re number in the range of 2000–9000, and heat flux in the range of 0.5–1.2 kW/m^2 as operating parameters. He emphasized that the corrugated surface had a significant effect on the increase in the heat transfer and pressure drop due to the presence of recirculation zones [11]. Tokgoz et al. investigated numerically and experimentally the flow properties and thermal efficiency in grooved duct geometries at the aspect ratios S/H = 0.1, 0.2, and 0.3. In their work, they examined the Reynolds numbers in the range of $3 \times 10^3 \leqslant \mathrm{Re} \leqslant 6 \times 10^3$. They stated that as the aspect ratio S/H grew, the heat transfer rate increased, having a maximum at S/H = 0.3, which corresponds to the highest aspect ratio. They also reported that the highest friction factor f occurred in the grooved channel with the aspect ratio S/H = 0.3, followed by S/H = 0.2 and 0.1 [12].

In literature, there are many studies aiming on enhancement of the heat transfer and flow. The main purpose of the present study is to investigate the turbulent flow and heat transfer over a triangular backward-facing step combined with a corrugated channel at different pitch lengths in comparison with a smooth structure. Numerical results were obtained for the Re number in the range of 5×10^3 to 2×10^4, channel step height of 10 mm, triangular surface amplitude height of 5 mm, and triangular surface step diameter of 5 mm, 10 mm, and 20 mm.

2. PHYSICAL MODELS AND METHOD

Schematic description of the backward-facing step geometry applied is illustrated in Fig. 1. The expansion ratio of the channel is 2 and the step size is H. The channel is divided into three main parts. The first is the part where the developed flow zone is created; the second is the test part where the heat flux is applied, and the third is the outlet part. The first part, which makes up one third of the channel length, is also called upstream, and the test and outlet parts, which make up two thirds, are called downstream.

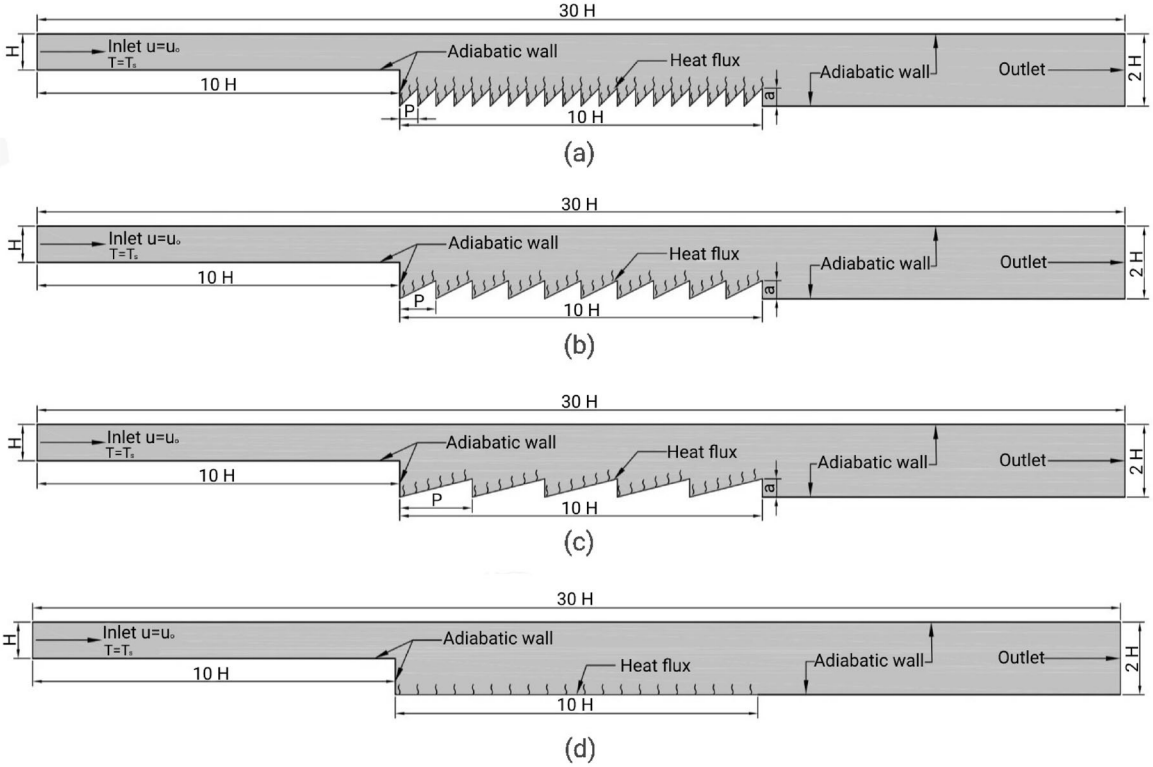

Fig. 1. Schematic view of studied model with boundary conditions: (a) p = 5 mm triangular heated surface; (b) p = 10 mm triangular heated surface; (c) p = 20 mm triangular heated surface; (d) smooth heated surface.

Table 1. Thermophysical properties of base fluid

Property	Fluid (water)
ρ (kg/m^3)	998
c_p (J/kg K)	4179
k (W/mK)	0.61
μ(kgm/s)	0.001003

The upstream length is 10 H, and the downstream length is 20 H. The main channel geometry has a smooth bottom surface, while the compared channel geometry has a triangular bottom surface with various pitch lengths (p = 5 mm, p = 10 mm, and p = 15 mm), and 4 kW/m^2 heat flux is applied to this surface. The other surfaces of the channel are adiabatic. At different Reynolds numbers (5×10^3, 10^4, 1.5×10^4, and 2×10^4), the flow velocity is defined in the inlet section and the outlet pressure is set in the outlet section. The fluid used is water; its properties are given in Table 1.

This study was conducted under the following assumptions.

- The corrugated channel flow field (2D) is two-dimensional, steady state, and turbulent.
- Incompressible water is used as the fluid to cool the triangle patterned surfaces.
- A constant heat flux of 4 kW/m^2 is used on the triangle patterned surfaces at the bottom of the channel.
- Except for the triangular pattern, the other surfaces are adiabatic.

The following governing equations used with these assumptions are solved with the use of Computational Fluid Dynamics (CFD).

Continuity equation

$$\frac{\partial \bar{\mathrm{u}}}{\partial \mathrm{x}} + \frac{\partial \bar{\mathrm{v}}}{\partial \mathrm{x}} = 0. \tag{1}$$

Momentum equation

x *direction momentum equation*

$$\left(\bar{\mathrm{u}}\frac{\partial \bar{\mathrm{u}}}{\partial \bar{\mathrm{x}}} + \frac{\partial \overline{(\mathrm{u}')^2}}{\partial \mathrm{x}}\right) + \left(\bar{\mathrm{v}}\frac{\partial \bar{\mathrm{u}}}{\partial \mathrm{y}} + \frac{\partial \overline{(\mathrm{u}'\mathrm{v}')}}{\partial \mathrm{y}}\right) = -\frac{1}{\rho}\frac{\partial \bar{\mathrm{p}}}{\partial \mathrm{x}} + \mathrm{v}\left(\frac{\partial^2 \bar{\mathrm{u}}}{\partial \mathrm{x}^2} + \frac{\partial^2 \bar{\mathrm{u}}}{\partial \mathrm{y}^2}\right), \tag{2}$$

y *direction momentum equation*

$$\left(\bar{\mathrm{u}}\frac{\partial \bar{\mathrm{v}}}{\partial \mathrm{x}} + \frac{\partial \overline{(\mathrm{v}')^2}}{\partial \mathrm{x}}\right) + \left(\bar{\mathrm{v}}\frac{\partial \bar{\mathrm{v}}}{\partial \mathrm{y}} + \frac{\partial \overline{(\mathrm{v}'\mathrm{v}')}}{\partial \mathrm{y}}\right) = -\frac{1}{\rho}\frac{\partial \bar{\mathrm{p}}}{\partial \mathrm{y}} + \mathrm{v}\left(\frac{\partial^2 \bar{\mathrm{v}}}{\partial \mathrm{x}^2} + \frac{\partial^2 \bar{\mathrm{v}}}{\partial \mathrm{y}^2}\right). \tag{3}$$

Energy equation

$$\left(\bar{\mathrm{u}}\frac{\partial \bar{\mathrm{T}}}{\partial \mathrm{x}} + \bar{\mathrm{v}}\frac{\partial \overline{\mathrm{T}}}{\partial \mathrm{y}}\right) + \left(\frac{\partial \overline{(\mathrm{u}'\mathrm{T}')}}{\partial \mathrm{x}} + \frac{\partial \overline{(\mathrm{v}'\mathrm{T}')}}{\partial \mathrm{y}}\right) = \frac{\mathrm{k}}{\rho \mathrm{c_p}} + \mathrm{v}\left(\frac{\partial^2 \bar{\mathrm{T}}}{\partial \mathrm{x}^2} + \frac{\partial^2 \bar{\mathrm{T}}}{\partial \mathrm{y}^2}\right) + \varphi. \tag{4}$$

The steady flow turbulence kinetic energy equation

$$\frac{\partial(\rho \mathrm{u}\mathrm{k}')}{\partial \mathrm{x}} + \frac{\partial(\rho \mathrm{v}\mathrm{k}')}{\partial \mathrm{y}} = \frac{\partial}{\partial \mathrm{x}}\left(\frac{\mu_\mathrm{t}}{\sigma_\mathrm{k}}\frac{\partial \mathrm{k}'}{\partial \mathrm{x}}\right) + \frac{\partial}{\partial \mathrm{y}}\left(\frac{\mu_\mathrm{t}}{\sigma_\mathrm{k}}\frac{\partial \mathrm{k}'}{\partial \mathrm{y}}\right) + \mu_\mathrm{t}\varphi - \rho\varepsilon. \tag{5}$$

Turbulence viscosity

$$\mu_{\mathrm{t}} = \mathrm{c}'_{\mu}\rho\frac{\mathrm{k}'^2}{\varepsilon}. \tag{6}$$

In the k-ε turbulence model used in the present study, ε indicates the turbulence distribution, while k′ and φ show the turbulence kinetic energy and viscous dissipation term, respectively.

Turbulence kinetic energy

$$\mathrm{k}' = \frac{1}{2}\left(\overline{\mathrm{u}'^2} + \overline{\mathrm{v}'^2} + \overline{\mathrm{w}'^2}\right). \tag{7}$$

Viscous dissipation term

$$\varphi = 2\mu\left[\left(\frac{\partial \mathrm{u}}{\partial \mathrm{x}}\right)^2 + \left(\frac{\partial \mathrm{v}}{\partial \mathrm{y}}\right)^2\right] + \mu\left(\frac{\partial \mathrm{v}}{\partial \mathrm{x}} + \frac{\partial \mathrm{u}}{\partial \mathrm{x}}\right)^2. \tag{8}$$

Turbulence kinetic energy disappearance equation

$$\frac{\partial(\rho \mathrm{u}\varepsilon)}{\partial \mathrm{x}} + \frac{\partial(\rho \mathrm{v}\varepsilon)}{\partial \mathrm{y}} + \frac{\partial(\rho \mathrm{w}\varepsilon)}{\partial \mathrm{z}} = \frac{\partial}{\partial \mathrm{x}}\left(\frac{\mu_{\mathrm{t}}}{\sigma_{\varepsilon}}\frac{\partial \varepsilon}{\partial \mathrm{x}}\right) + \frac{\partial}{\partial \mathrm{y}}\left(\frac{\mu_{\mathrm{t}}}{\sigma_{\varepsilon}}\frac{\partial \varepsilon}{\partial \mathrm{y}}\right) + \frac{\partial}{\partial \mathrm{z}}\left(\frac{\mu_{\mathrm{t}}}{\sigma_{\varepsilon}}\frac{\partial \varepsilon}{\partial \mathrm{z}}\right)$$

$$+\mathrm{C}_{1\varepsilon}\mu_{\mathrm{t}}\frac{\varepsilon}{\mathrm{k}'}\varphi - \mathrm{C}_{2\varepsilon}\rho\frac{\varepsilon^2}{\mathrm{k}'}. \tag{9}$$

The model constants C_{μ}, $\mathrm{C}_{1\varepsilon}$, $\mathrm{C}_{2\varepsilon}$, σ_k, and σ_{ε} are typical default values used in the standard k-ε turbulence model [18]. The values of these constants have resulted from numerous data fitting iterations for many turbulent flows.

Calculation of the Re number is done with the equation

$$\mathrm{Re} = \frac{\rho \mathrm{V}_{\infty}\mathrm{D}_{\mathrm{h}}}{\mu}. \tag{10}$$

D_h is called the hydraulic diameter of the flow inlet and is calculated as follows:

$$\mathrm{D}_{\mathrm{h}} = \frac{4\mathrm{A}_{\mathrm{c}}}{\mathrm{P}}. \tag{11}$$

In this hydraulic diameter equation, A_{c} is the cross-sectional area and P is the length of the inlet perimeter.

The Nu number is considered as the ratio of the convection heat transfer rate to the conduction heat transfer rate. The local Nu number is calculated as follows:

$$-\mathrm{k}\left(\frac{\partial \mathrm{T}}{\partial \mathrm{n}}\right)_{\mathrm{s}} = \mathrm{h}\left(\mathrm{T}_{\infty} - \mathrm{T}_{\mathrm{s}}\right) \ \text{ and } \ \mathrm{Nu} = \frac{\mathrm{hD}_{\mathrm{h}}}{\mathrm{k}}. \tag{12}$$

Here h is the local heat transfer coefficient on the surface and n is the direction perpendicular to the surface.

The mean heat transfer coefficient calculation:

$$\mathrm{h}_{\mathrm{m}} = \frac{1}{\mathrm{L}}\int_0^{\mathrm{L}} \mathrm{h}\mathrm{d}\mathrm{x}. \tag{13}$$

The mean Nu number calculation:

$$\mathrm{Nu_m} = \frac{\mathrm{h_m D_h}}{\mathrm{k}}. \tag{14}$$

One of the most important steps to ensure the accuracy of the study is through mesh independence. For mesh independence, a certain output parameter is considered for analysis and compared at different numbers of nodes or elements. The output parameter selected in the study is the average Nusselt number. The analysis is done for the Reynolds number Re = 5000 with the main channel geometry with the straight bottom surface. The first mesh structure has a number of 1212 elements with a curvature grid. The Nusselt number obtained for this number of elements is 34.4. The number of elements is increased periodically, and the graph in Fig. 2 is created. It is clearly seen that the average Nu number goes horizontally at Nu = 50 after 120000 elements. This situation can be used for the model created with 120000 or more elements and proves the fact that the results are acceptable. The study is continued with 164916 elements. In addition, the results obtained for Re = 5000 are compared with the experimental results of Elshafei EAM et al. [13] and the results of the numerical study by Ali Kareem Hilo et al. (Nu = 51) [14] in the literature. The mesh structure used in the study is shown in Fig. 3 for a 20 mm triangular structure. Inflation is also applied to the surfaces.

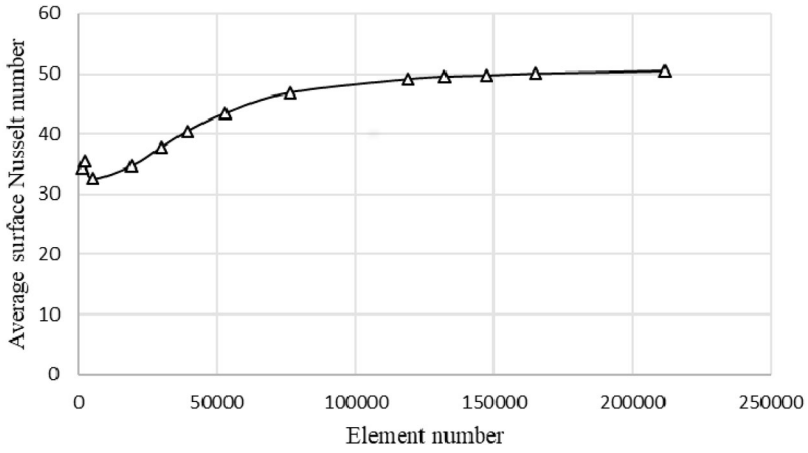

Fig. 2. Mesh independence with element number—average surface Nusselt number.

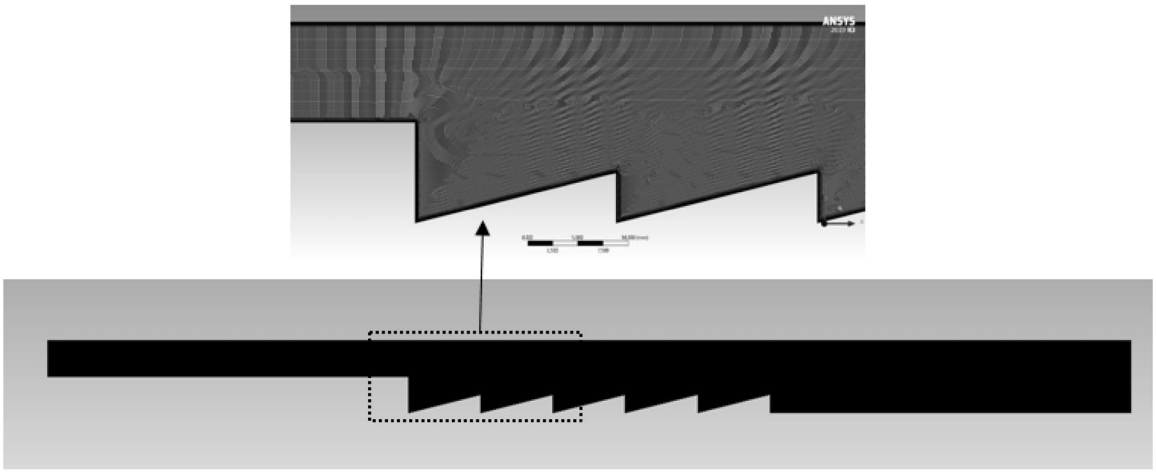

Fig. 3. Mesh structure and detail view.

3. RESULTS

In the present numerical study, the Reynolds number Re for a backward step flow with a constant heat flux is studied in the range of 5000 to 20000. The effects of the triangular structure and the Re number on the thermal and hydraulic performance are presented and interpreted in this section. The results obtained in this study are supported by previous studies, as discussed briefly.

The effects of different corrugation shapes on the velocity distribution are shown in Figs. 4–7 for different Reynolds numbers. As can be seen from the figures, the recirculation zone starts to form at the test part step corner on the straight bottom surfaces, and a single vortex area occurs. This is consistent with the results in the literature on a fluid flow through a backward step channel [5, 11, 13]. However, the tip and base portion of the corrugation shapes play an important role in the velocity streamline. The triangular surfaces reduce the length of the main recirculation by disrupting the main recirculation of the flow immediately after the back step (e.g., compare Fig. 4a with Figs. 4b, 4c, or 4d). In addition, the triangular surfaces form a stable vortex in the corrugated part of each shape by dividing the single vortex that appears on the straight surface. In addition, the joining portion of the triangular corrugated walls leads to a thinner thermal boundary layer. The velocity streamlines near walls are always low due to the friction between the viscous substrates and the wall. However, the use of corrugated walls in the backward facing step channel increases the velocity distribution near the wall and this results in better mixing of the flow layers.

Figures 8–11 give the turbulent kinetic energy distributions at different Reynolds numbers for the straight bottom surface and triangular grooved bottom surfaces with different pitch lengths. This distribution extends over a wider area for the straight bottom surface. The triangular surfaces disperse this area, revealing smaller and maximum points in contact with each other. In addition, the maximum TKE values obtained grow with increase in the Reynolds number. While the TKE values for Re = 5000 are around 0.02 m^2/s^2, this value is 0.27 m^2/s^2 at Re = 20000.

The combination of corrugated wall with the backward face step has a significant effect on the fluid flow and heat transfer, as shown in Figs. 12a and 12b, which present the surface Nusselt number Nu and the skin friction coefficient at the surface. The graph results for each Re number studied are comparatively given for the straight, 5 mm triangular, 10 mm triangular, and 20 mm triangular cases. It is seen that the Nu number is multivariate along the x axis for a triangular grooved bottom as compared

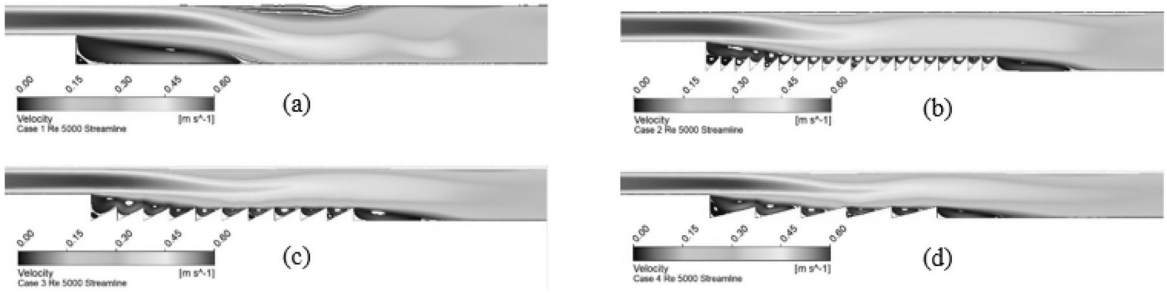

Fig. 4. Velocity streamlines through backward-facing step with Re = 5000 for (a) straight bottom, (b) p = 5 mm triangular bottom, (c) p = 10 mm triangular bottom, and (d) p = 20 mm triangular bottom.

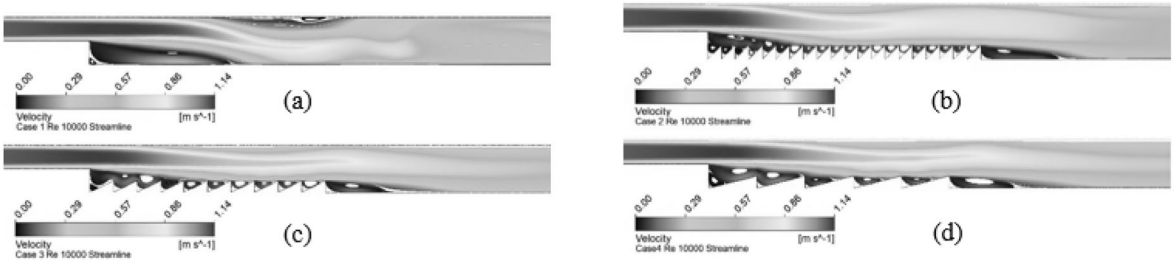

Fig. 5. Velocity streamlines through backward-facing step with Re = 10000 for (a) straight bottom, (b) p = 5 mm triangular bottom, (c) p = 10 mm triangular bottom, and (d) p = 20 mm triangular bottom.

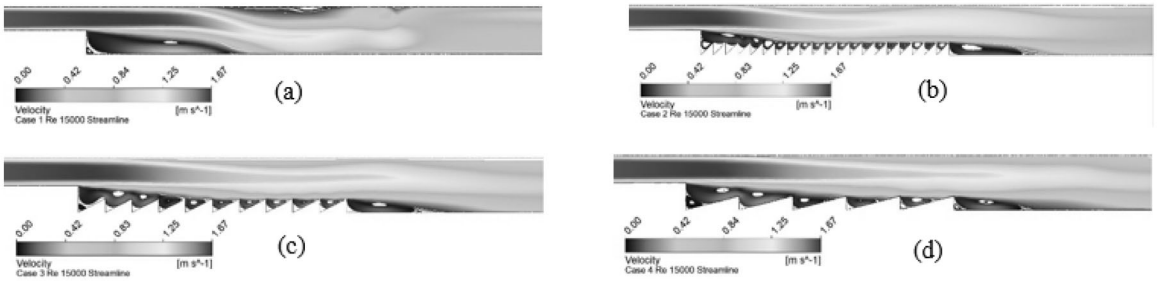

Fig. 6. Velocity streamlines through backward-facing step with Re = 15000 for (a) straight bottom, (b) p = 5 mm triangular bottom, (c) p = 10 mm triangular bottom, and (d) p = 20 mm triangular bottom.

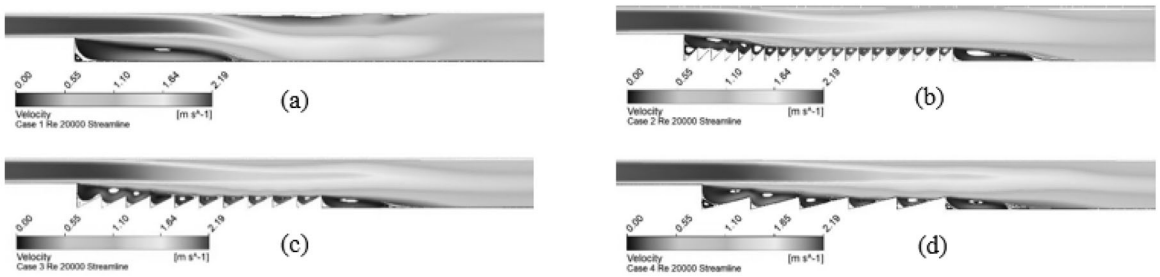

Fig. 7. Velocity streamlines through backward-facing step with Re = 20000 for (a) straight bottom, (b) p = 5 mm triangular bottom, (c) p = 10 mm triangular bottom, and (d) p = 20 mm triangular bottom.

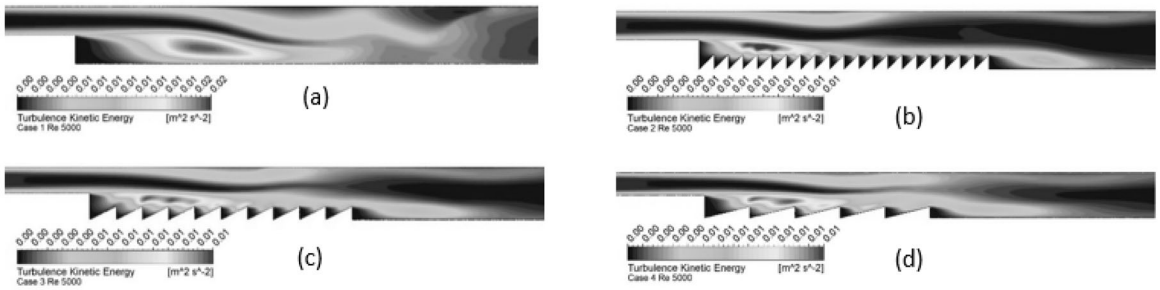

Fig. 8. TKE distribution through backward-facing step with Re = 5000 for (a) straight bottom, (b) p = 5 mm triangular bottom, (c) p = 10 mm triangular bottom, and (d) p = 20 mm triangular bottom.

with the straight bottom shape. It is observed that the Nusselt number peak values are the highest for 5 mm and then 10 mm triangular and 20 mm triangular bottom surfaces and the lowest for the straight bottom. In addition, as expected, the skin friction values on the straight bottom surface are lower than those on the other surfaces. This is a possible situation. The aim of such studies is to enhance the heat transfer with the effect of pressure drop at a certain rate. When the skin friction graphs given in Fig. 12b are examined, the most remarkable part is the minimum level after the peak at a certain distance for the straight-bottomed model. While this point is at 0.02 m distances at Re = 5000, it moves further in the x axis with increase in the Re number. This situation arises from the flow separation and the recirculation zone after the inlet section. After the recirculation zone, the skin friction grows again. In addition, it is clearly seen from the graph values that the Nusselt number increases and the skin friction values decrease with the growth of the Reynolds number.

In addition, Fig. 12 shows that the surface Nusselt number and skin friction coefficient distributions of all the triangular grooved surfaces differ from those of the straight base surface, the highest and lowest values occurring exactly at the location of the lowest and highest section of the triangular shape. The increase in the heat transfer is associated with the flow problem, and the flow over the triangular corrugated base creates multiple recirculation zones and thin boundary layers. This indicates that the

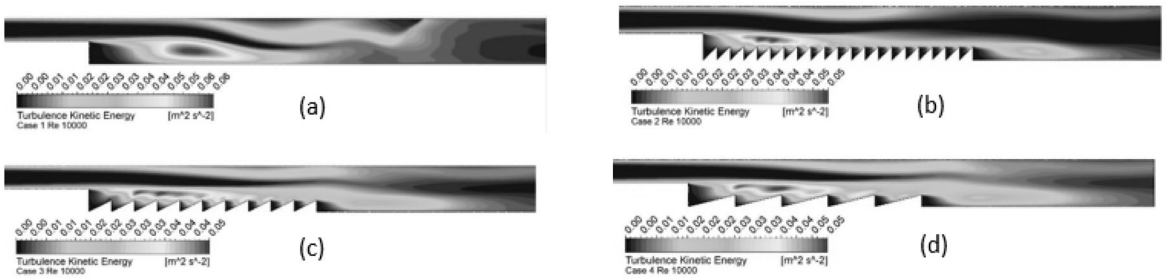

Fig. 9. TKE distribution through backward-facing step with Re = 10000 for (a) straight bottom, (b) p = 5 mm triangular bottom, (c) p = 10 mm triangular bottom, and (d) p = 20 mm triangular bottom.

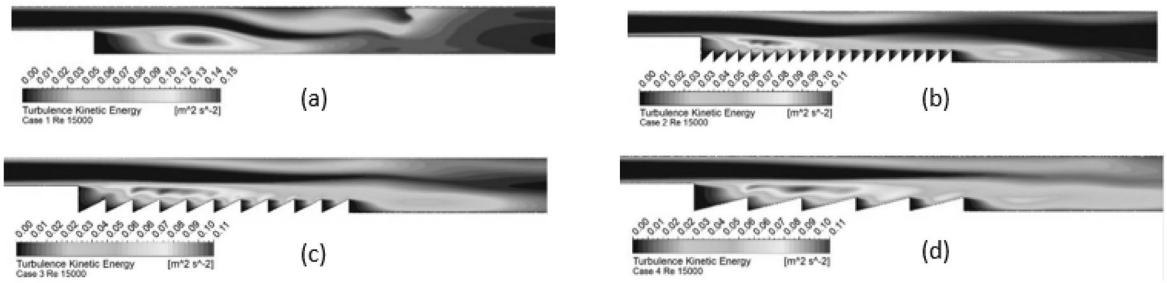

Fig. 10. TKE distribution through backward-facing step with Re = 15000 for (a) straight bottom, (b) p = 5 mm triangular bottom, (c) p = 10 mm triangular bottom, and (d) p = 20 mm triangular bottom.

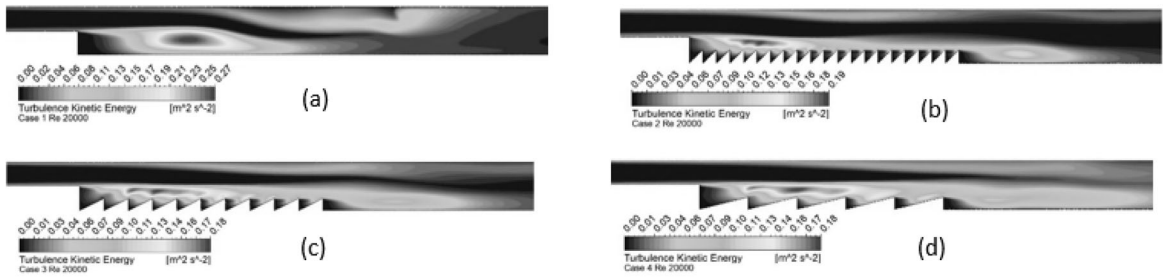

Fig. 11. TKE distribution through backward-facing step with Re = 20000 for (a) straight bottom, (b) p = 5 mm triangular bottom, (c) p = 10 mm triangular bottom, and (d) p = 20 mm triangular bottom.

triangular grooved surface is more effective with the backward step and creates better heat transfer. Further, Fig. 12a shows that Nu is higher in the convergent portion of each wave of the corrugation shape than in the diverging portion. The main reason for this situation is that the velocity gradient and the average velocity of the convergent section are higher, resulting in increase in the heat transfer rate. Nu is almost constant after the third fluctuation of the channel with each triangular base. In other words, in the triangular-base channels, the same fluctuations in the Nusselt number occur after around the 0.02 m distance in the x axis.

In addition to the surface Nusselt number and skin friction coefficient variation along the x axis, given in Fig. 12, their mean values are presented in Table 2, as well as the graphs in Fig. 13. As the Re number increases, the average Nu number grows for all the surfaces, while the average skin friction coefficient values decrease. The highest mean Nu number occurs in the channel with the 5 mm triangular base surface. This is due to the smaller vortex areas on the 5 mm triangular surface. With the growth of the vortex recirculation area, the mean Nu numbers also increase in the channels with the 10 mm triangular surface and 20 mm triangular surface. The highest mean Nu number (109.63) at Re = 5000 is observed in the model with the 5 mm triangular surface. Despite its effect of the heat transfer enhancement, the skin friction value has the highest value in the 5 mm triangular surface channel, as seen in Table 2.

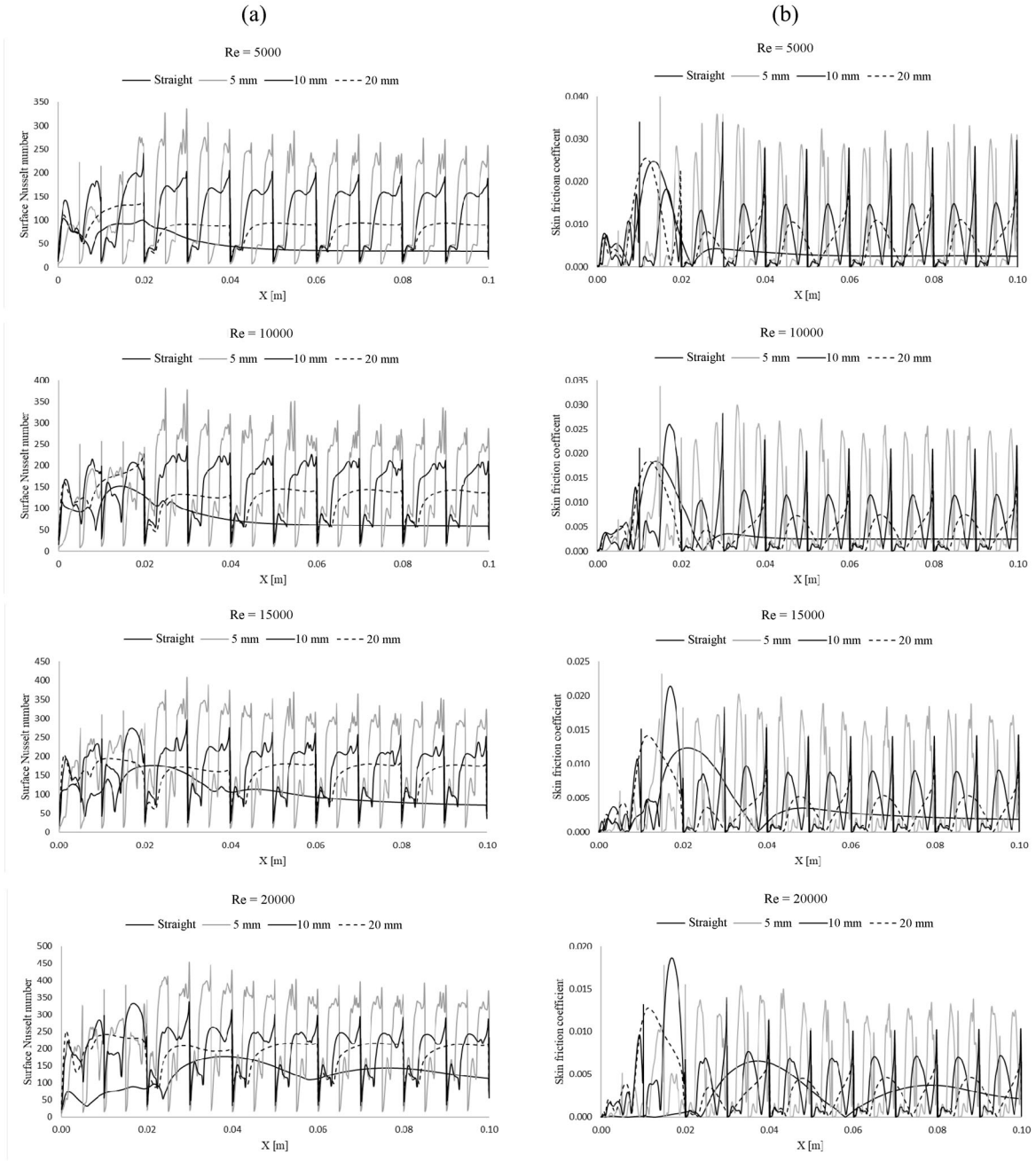

Fig. 12. (a) Surface Nusselt number and (b) skin friction coefficient distributions.

The pressure drop and fluid temperature increase values for channels with different bottom surfaces are given in Table 3 and graphically presented in Fig. 14. As can be clearly seen from Fig. 14b, although the highest temperature is obtained in the channel with the 5 mm triangular surface, the Performance Evaluation Criterion (PEC) is the lowest model due to the higher pressure drop and the higher friction factor. In all the models, the pressure difference increases and the temperature difference decreases between the channel inlet and outlet with the Re number growing.

The increase in the pressure drop is related to the augmentation of the heat transfer. Therefore, it is very important to explain the efficiency of corrugated surface using the Performance Evaluation Criterion (PEC). Higher PEC values provide higher heat transfer. Furthermore, a PEC value greater

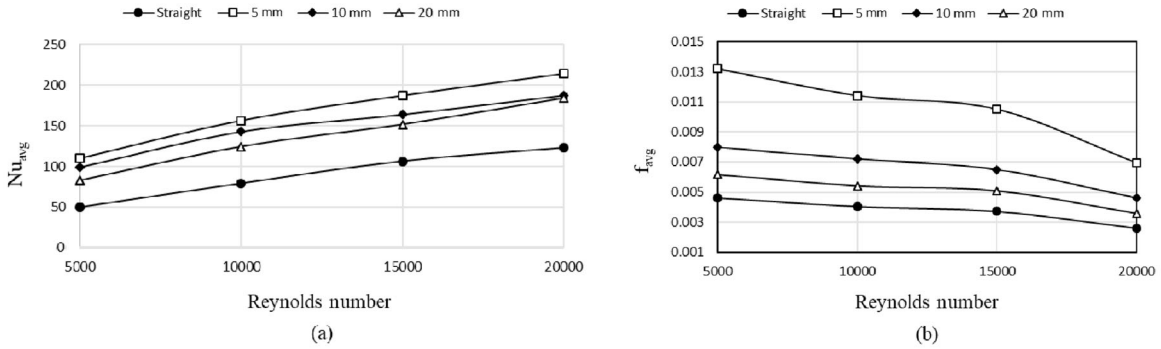

Fig. 13. (a) Average Nu number and (b) average skin friction coefficient for different Re numbers.

Table 2. Values obtained at different Re numbers for different channel surfaces

	Average Nusselt number (Nu_{avg})				Average skin friction coefficient (f_{avg})			
Re	Straight	5 mm	10 mm	20 mm	Straight	5 mm	10 mm	20 mm
5000	50.27	109.63	99.02	82.92	0.00463	0.0132	0.00798	0.00615
10000	79.3623	156.15	142.61	124.27	0.00405	0.01142	0.00721	0.00541
15000	106.485	186.76	163.68	151.47	0.00372	0.01051	0.00649	0.00508
20000	122.681	213.85	187.04	183.59	0.00261	0.00695	0.00459	0.00359

Table 3. Pressure and temperature values obtained at different Re numbers

	Straight		5 mm		10 mm		20 mm	
Re	ΔP (Pa)	ΔT (°C)	ΔP (Pa)	ΔT (°C)	ΔP (Pa)	ΔT (°C)	ΔP (Pa)	ΔT (°C)
5000	21.332	0.019	25.192	0.046	22.138	0.031	22.734	0.025
10000	129.781	0.009	151.551	0.023	142.771	0.015	135.345	0.012
15000	330.051	0.006	386.325	0.015	351.965	0.010	355.812	0.008
20000	626.516	0.005	690.696	0.011	672.717	0.008	681.479	0.006

than 1 indicates that the heat transfer rate exceeds the increase in the pressure drop [15–17]. The PEC values are obtained as follows:

$$\mathrm{PEC} = \frac{\mathrm{Nu}/\mathrm{Nu_o}}{\mathrm{f}/\mathrm{f_o^{1/3}}}. \tag{15}$$

Here Nu and f represent the mean Nusselt number and average skin friction coefficient values for the evaluated surface, while Nu_o and f_o represent the mean Nusselt number and average skin friction coefficient value for the straight surface.

The effect of triangular surfaces with different pitch lengths on the PEC is shown in Fig. 15 for different Re numbers. The PEC values are also presented in Table 4. The PEC values vary with increasing Re number due to the Nu number and the skin friction effect. Initially, the PEC value for all models decreases for Re of up to 15000, while a slight increase is observed at Re = 20000. The maximum PEC value occurs on the triangular surface with a pitch length of 10 mm, and a high decrease is observed with the augmentation in the Re number due to the increase in the friction factor and the limited increase in Nu. The PEC value for the 20 mm pitch triangular surface follows a more stable path

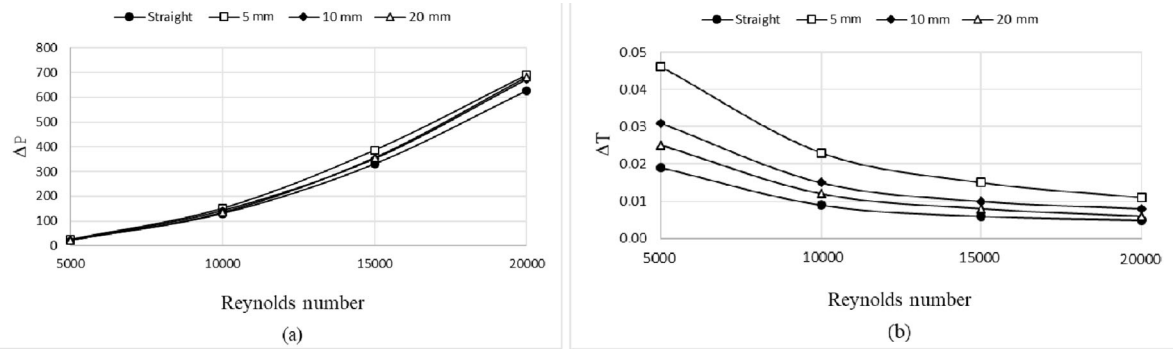

Fig. 14. (a) Pressure drop and (b) temperature increase vs. Re number.

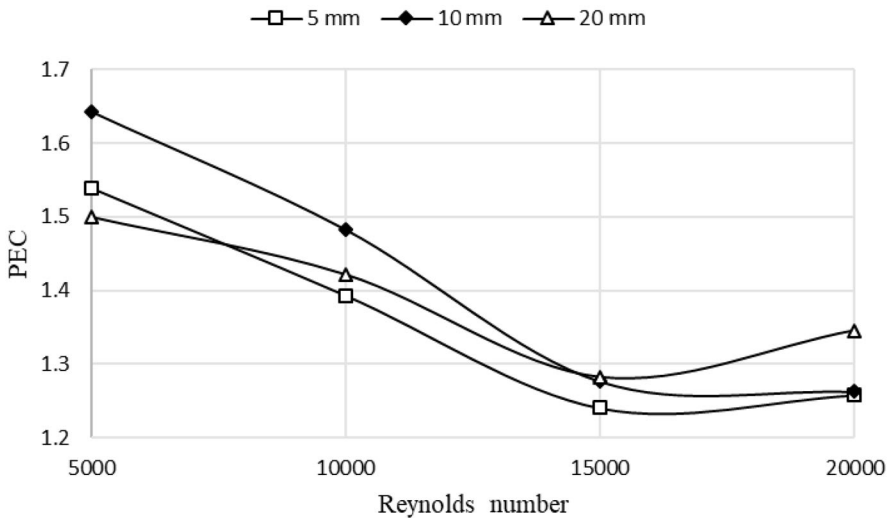

Fig. 15. PEC change for different Re numbers.

Table 4. PEC values obtained at different Re numbers

Re	5 mm triangular	10 mm triangular	20 mm triangular
5000	1.537984	1.64262	1.500226
10000	1.392794	1.482736	1.421838
15000	1.240547	1.276924	1.282057
20000	1.25783	1.262762	1.345695

compared with the other shapes due to the significant increase in the heat transfer. Besides, the most effective Re number in terms of PEC values is 5000.

4. CONCLUSION

In this study, numerical simulations of turbulent flow with different groove bottoms with backward step are analyzed and discussed. The effects of corrugated design on heat transfer enhancement at a constant heat flux are investigated. The hydraulic diameter of the corrugated wall is kept constant. The main objective is improving the heat transfer, which includes different parameters such as the pitch length of triangular grooved shape and Reynolds number Re.

The results show that the triangular surfaces enhance the heat transfer over the backward-facing step channel. It is observed that triangular shapes with different pitch lengths significantly affect the

performance evaluation criterion, which is a factor of the Nusselt number Nu and friction. It is also concluded that a smaller pitch length leads to a higher heat transfer rate and has a significant effect on the surface skin friction factor. As Re grows, the Nu number increases and the surface friction coefficient decreases. The best improvement in the heat transfer rate by the backward step at Re = 5000 and a triangular pitch length of 10 mm is obtained with a slotted base. This situation was evaluated at PEC = 1.64. It has been concluded that this situation is more effective with higher Nu and low skin friction for the channel with the 20 mm bottom surface with increase in the Re number.

NOTATIONS

A—area
a—amplitude of corrugation (mm)
p—pitch of corrugation (mm)
D_h—hydraulic diameter
f—friction factor,
h—convection coefficient ($W/m^2 \cdot K$)
H—height of channel (mm)
V—flow velocity
P—pressure
T—temperature
Nu—Nusselt number
Re—Reynolds number
CFD—Computational Fluid Dynamic
FVM—Finite Volume Method
PEC—Performance Evaluation Criterion
TKE—Turbulence Kinetic Energy

REFERENCES

1. Wang, C. and Chen, C., Forced Convection in a Wavy-Wall Channel, *Int. J. Heat Mass Transfer*, 2002, vol. 45, pp. 2587–2595.
2. Hassanzadeh, R. and Tokgoz, N., Thermal-Hydraulic Characteristics of Nano Fluid Flow, *J. Eng. Therm.*, 2017, vol. 26, no. 4, pp. 498–513.
3. Ahmed, M.A., Shuaib, N.H., and Yusoff, M.Z., Numerical Investigations of Flow and Heat Transfer Enhancement in a Corrugated Channel Using Nano Fluid, *Int. Comm. Heat Mass Transfer*, 2011, vol. 38, pp. 1368–1375.
4. Akbarzadeh, M. and Maghrebi, M.J., Combined Effects of Corrugated Walls and Porous Inserts on Performance Improvement in a Heat Exchanger Channel, *Int. J. Therm. Sci.*, 2018, vol. 127, pp. 266–276.
5. Khoshvaght-aliabadi, M., Influence of Different Design Parameters and Al_2O_3-Water Nanofluid Flow on Heat Transfer and Flow Characteristics of Sinusoidal-Corrugated Channels, *Energy Convers. Manag.*, 2014, vol. 88, pp. 96–105.
6. Sakr, M., Convective Heat Transfer and Pressure Drop in V-Corrugated Channel with Different Phase Shifts, *Heat Mass Transfer*, 2015, vol. 51, pp. 129–141.
7. Savino, S., Comini, G., and Nonino, C., Three-Dimensional Analysis of Convection in Two-Dimensional Wavy Channels, *Numer. Heat Transf. Part A: Appl.*, 2010, vol. 7782, no. 46, pp. 869–890.
8. Mahmud, S., Separation Characteristics of Fluid Flow Inside Two Parallel Plates with Wavy Surface, *Int. J. Eng. Sci.*, 2002, vol. 40, pp. 1495–1509.
9. Ali, M.M. and Ramadhyani, S., Experiments on Convective Heat Transfer in Corrugated Channels, *Exp. Heat Transfer*, 2007, vol. 5, no. 3, pp. 175–193.
10. Islamoglu, Y. and Parmaksızoglu, C., The Effect of Channel Height on the Enhanced Heat Transfer Characteristics in a Corrugated Heat Exchanger Channel, *Appl. Therm. Eng.*, 2003, vol. 23, pp. 979–987.
11. Naphon, P., Heat Transfer Characteristics and Pressure Drop in Channel with V Corrugated Upper and Lower Plates, *Energy Convers. Manag.*, 2007, vol. 48, pp. 1516–1524.
12. Tokgoz, N., Aksoy, M.M., and Sahin, B., Investigation of Flow Characteristics and Heat Transfer Enhancement of Corrugated Duct Geometries, *Appl. Therm. Eng.*, 2017, vol. 118, pp. 518–530.

13. Elshafei, E.A.M., Awad, M.M., and Ali, A.G., Heat Transfer and Pressure Drop in Corrugated Channels, *Energy*, 2010, vol. 35, no. 1, pp. 101–110.
14. Kareem, A., et al., Effect of Corrugated Wall Combined with Backward-Facing Step Channel on Fluid Flow and Heat Transfer, *Energy*, 2020, vol. 190, p. 116294.
15. Manca, O., Nardini, S., and Ricci, D., A Numerical Study of Nano Fluid Forced Convection in Ribbed Channels, *Appl. Therm. Eng.*, 2012, vol. 37, pp. 280–292.
16. Pina, A., Ferrão, P., Fournier, J., Lacarriére, B., and Le Corre, O., Heat Transfer Enhancement of a Molten Salt Parabolic Trough Solar Receiver with Concentric and Eccentric Pipe Inserts, *Energy Procedia*, 2017, vol. 142, pp. 624–629.
17. Webb, R.L., *Principles of Enhanced Heat Transfer*, John Willey and Sons, Chichester, 1994.